Planetary and Space Science 137 (2017) 32–39

Contents lists available at ScienceDirect

Planetary and Space Science

journal homepage: www.elsevier.com/locate/pss

A desktop system of virtual morphometric globes for Mars and the Moon

I.V. Florinsky*, S.V. Filippov

Institute of Mathematical Problems of Biology, the Keldysh Institute of Applied Mathematics, Russian Academy of Sciences, Pushchino, Moscow Region 142290, Russia

ARTICLE INFO

Keywords:
Geomorphometry
3D modeling
3D visualization
Digital elevation model
Digital terrain model

ABSTRACT

Global morphometric models can be useful for earth and planetary studies. Virtual globes — programs implementing interactive three-dimensional (3D) models of planets — are increasingly used in geo- and planetary sciences. We describe the development of a desktop system of virtual morphometric globes for Mars and the Moon. As the initial data, we used 15'-gridded global digital elevation models (DEMs) extracted from the Mars Orbiter Laser Altimeter (MOLA) and the Lunar Orbiter Laser Altimeter (LOLA) gridded archives. For two celestial bodies, we derived global digital models of several morphometric attributes, such as horizontal curvature, vertical curvature, minimal curvature, maximal curvature, and catchment area. To develop the system, we used Blender, the free open-source software for 3D modeling and visualization. First, a 3D sphere model was generated. Second, the global morphometric maps were imposed to the sphere surface as textures. Finally, the real-time 3D graphics Blender engine was used to implement rotation and zooming of the globes. The testing of the developed system demonstrated its good performance. Morphometric globes clearly represent peculiarities of planetary topography, according to the physical and mathematical sense of a particular morphometric variable.

1. Introduction

Topography is one of the fundamental characteristics of a planetary body. In this connection, methods of geomorphometry are widely used to solve various multiscale problems of geosciences (Moore et al., 1991; Wilson and Gallant, 2000; Li et al., 2005; Hengl and Reuter, 2009; Florinsky, 2016). Geomorphometry is a science of quantitative modeling and analysis of the topographic surface and relationships between topography and other natural components of geosystems. Properties of the topographic surface are described by morphometric variables, such as horizontal curvature (k_h), vertical curvature (k_v), minimal curvature (k_{min}), maximal curvature (k_{max}), catchment area (CA), etc. (Table 1). Geomorphometric modeling and mapping allow one to describe geometry of landforms, to quantify topographic prerequisites of gravity-driven overland and intrasoil lateral transport of liquids (water and/or other substances), and to reveal or delineate topographically expressed endo- and exogenic structures (e.g., lineaments, destroyed craters, palaeo-channels, palaeo-deltas).

Notice that morphometric variables describe a surface in gravity regardless of the surface origin and the existence of water or other liquids on the surface. Geomorphometric modeling is associated with the concept of general geomorphometry, which is defined as "the measurement and analysis of those characteristics of landform which are applicable to any continuous rough surface…. General geomorphometry as a whole provides a basis for the quantitative comparison even of qualitatively different landscapes, and it can adapt methods of surface analysis used outside geomorphology" (Evans, 1972, p. 18). Thus, although geomorphometric methods were originally focused on terrestrial landscapes, they can be naturally applied to study extraterrestrial topography.

In the last years, significant progress has been made in the development and application of virtual globes (Tuttle et al., 2008; Kennedy, 2009; Blaschke et al., 2012). Virtual globes are programs implementing interactive three-dimensional (3D) models of celestial bodies. The list of virtual globes includes World Wind (NASA, 2003–2011), Earth3D (Gunia, 2004–2015), Google Earth (Google, 2005–2014), Marble (KDE, 2007–2014), Cesium (AGI, 2012–2015), and others. Virtual globes enable to carry out 3D multi-scale visualization of complex spatially distributed multi-layer data with capabilities to move around the globe and to change the user viewing angle and position relative to the globe. Virtual globes are increasingly used to solve various tasks of geosciences at various spatial scales (Chen and Bailey, 2011; Paraskevas, 2011; Guth, 2012; Whitmeyer et al., 2012; Yu and Gong, 2012; Zhu et al., 2014, 2016; Scheffers et al., 2015; Müller et al., 2016).

Global morphometry of the Earth and other celestial bodies can be useful for earth and planetary studies (Cazenave et al., 1989; Solomon et al., 1991; Graham et al., 1999; Smith et al., 1999; Vörösmarty et al.,

* Corresponding author.
E-mail address: iflor@mail.ru (I.V. Florinsky).

http://dx.doi.org/10.1016/j.pss.2017.01.005
Received 8 November 2016; Received in revised form 22 December 2016; Accepted 10 January 2017
Available online 11 January 2017

Table 1
Definitions and interpretations of some morphometric variables (Shary et al., 2002; Florinsky, 2016, chap. 2).

Variable (unit)	Definition and interpretation
Horizontal (tangential) curvature, k_h (m^{-1})	k_h is the curvature of a normal section tangential to a contour line at a given point of the topographic surface. k_h is a measure of flow convergence (the first mechanism of flow accumulation): gravity-driven overland and intrasoil lateral flows are converged where $k_h < 0$, and they are diverged where $k_h > 0$. Geomorphologically, k_h mapping allows revealing ridge and valley spurs (divergence and convergence areas, correspondingly), which combination reveals so-called flow structures.
Vertical (profile) curvature, k_v (m^{-1})	k_v is the curvature of a normal section having a common tangent line with a slope line at a given point of the topographic surface. A measure of relative deceleration and acceleration of gravity-driven flows (the second mechanism of flow accumulation). Overland and intrasoil lateral flows are decelerated where $k_v < 0$, and they are accelerated where $k_v > 0$ Geomorphologically, k_v mapping allows revealing terraces and scarps.
Minimal curvature, k_{min} (m^{-1})	k_{min} is a curvature of a principal section with the lowest value of curvature at a given point of the topographic surface. Geomorphologically, positive values of k_{min} correspond to local convex landforms, while its negative values relate to valleys.
Maximal curvature, k_{max} (m^{-1})	k_{max} is a curvature of a principal section with the highest value of curvature at a given point of the topographic surface Geomorphologically, positive values of k_{max} correspond to ridges, while its negative values relate to local concave landforms.
Catchment area, *CA* (m^2)	*CA* is an area of a closed figure formed by a contour segment at a given point of the topographic surface and two flow lines coming from upslope to the contour segment ends. *CA* is a measure of the contributing area. Geomorphologically, *CA* mapping allows revealing ridge and thalweg networks.

2000; Wieczorek, 2007; Florinsky, 2008a, 2008b; Willner et al., 2014; Karachevtseva et al., 2014, 2015; Wählisch et al., 2014). In virtual globes, it is a common practice to visualize topography using three popular cartographic approaches: (a) hypsometric tinting, (b) analytical hill shading, and (c) color relief shading (Cozzi and Ring, 2011, pt. 4). In hypsometric tinting, a topographic surface is subdivided into a set of elevation value intervals; each interval is assigned a color, shade of color, or shade of gray from a color scale, monochromic scale, or gray scale, correspondingly. In analytical hill shading, reflectance – a measure of the brightness of an illuminated surface – is estimated and mapped with various models of light reflectance from a surface, such as the Lambertian model, Lommel–Seeliger law, Minnaert function, and others (Horn, 1981). Color relief shading combines hypsometric tinting and hill shading (Jenny and Hurni, 2006). For example, this approach is utilized in Mars and the Moon globes based on the Google Earth engine (Google, 2005–2014). However, there do not exist virtual globes displaying terrain peculiarities described in terms of other morphometric variables (e.g., k_h, k_v, k_{min}, k_{max}, and *CA*).

Virtual globes utilize engines usually developed with 3D graphics application programming interface (API), such as OpenGL and WebGL (Cozzi and Ring, 2011). Rapid zooming of massive datasets is commonly provided by hierarchical tessellation of the globe surface (Mahdavi-Amiri et al., 2015). However, a level of complexity of rendering data should be considered in developing new virtual globes, in particular, in selection of the existing engine or development of a new one. Specialized multifunctional engines are not necessarily required for some relatively simple tasks.

Indeed, 3D scientific visualization can be carried out using the capabilities of the existing 3D graphics packages (Filippov and Sobolev, 2002; Hansen and Johnson, 2005; Lipşa et al., 2012; Johnson and Hertig, 2014). In particular, Blender — the free and open-source software for 3D modeling, visualization, and animation (Blender Foundation, 2003–2015; Hess, 2010; Blain, 2014) — is currently applied for 3D scientific visualization (Kent, 2015), e.g., in biology (SciVis, 2011–2015; Autin et al., 2012), astronomy (Kent, 2013), and geoinformatics (Scianna, 2013).

In this paper we describe the development of a desktop system of virtual morphometric globes for Mars and the Moon using Blender.

2. Data and methods

The system development consisted of two main steps:

1. Derivation of a set of global morphometric maps for Mars and the Moon.
2. 3D modeling of morphometric globes.

2.1. Digital terrain modeling

To facilitate the development of the desktop system of virtual morphometric globes, we decided to work with low resolution models. As the initial data, we used the following 15'-gridded global digital elevation models (DEMs):

- A DEM of Mars extracted from the Mars Orbiter Laser Altimeter (MOLA) gridded data record archive (Smith et al., 1999, 2003).
- A DEM of the Moon extracted from the Lunar Orbiter Laser Altimeter (LOLA) gridded data record archive (Neumann, 2008; Smith et al., 2010).

Any DEM includes high-frequency noise leading to the derivation of useless, noisy digital models and unreadable maps of morphometric variables (Florinsky, 2002). The problem can be partially resolved by DEM smoothing. To suppress high-frequency noise, the DEMs were smoothed using a 3×3 moving window. The Mars and Moon DEMs were twice and thrice smoothed, correspondingly. The number of smoothing was chosen empirically to provide visually smooth and readable patterns on global morphometric maps.

For Mars and the Moon, we derived global digital models of several morphometric attributes — k_h, k_v, k_{min}, k_{max}, and *CA* (Table 1) — from the smoothed DEMs. We chose these variables due to the following reasons. First, k_h, k_v, k_{min}, and k_{max} are most important local morphometric variables describing the surface geometry in the vicinity of a given point of the surface. k_h modeling allows to map systems of ridge and valley spurs, which combinations can form 'flow structures' associated with modern and palaeo-drainage network, lava flow systems, and the like. k_v mapping allows to reveal, in particular, terraces and scarps. k_{min} modeling allows to map valleys and local convex landforms. k_{max} mapping allows to reveal ridges and local concave landforms. Second, *CA* is the most important nonlocal morphometric variable characterizing a relative position of a given point on the surface. *CA* modeling allows to map, in particular, ridge and thalweg networks.

Local morphometric variables were calculated by the following equations (Shary et al., 2002; Florinsky, 2016, chap. 2):

$$k_h = -\frac{q^2 r - 2pqs + p^2 t}{(p^2 + q^2)\sqrt{1 + p^2 + q^2}}, \quad (1)$$

$$k_v = -\frac{p^2 r + 2pqs + q^2 t}{(p^2 + q^2)\sqrt{(1 + p^2 + q^2)^3}}. \quad (2)$$

$$k_{\min} = H - \sqrt{H^2 - K}, \quad (3)$$

$$k_{max} = H + \sqrt{H^2 - K}, \quad (4)$$

where H and K are mean and Gaussian curvatures, correspondingly:

$$H = -\frac{(1+q^2)r - 2pqs + (1+p^2)t}{2\sqrt{(1+p^2+q^2)^3}}, \quad (5)$$

$$K = \frac{rt - s^2}{(1+p^2+q^2)^2}, \quad (6)$$

p, q, r, s, and t are the first and second partial derivatives of elevation (z):

$$p = \frac{\partial z}{\partial x}, \; q = \frac{\partial z}{\partial y}, \; r = \frac{\partial^2 z}{\partial x^2}, \; s = \frac{\partial^2 z}{\partial x \partial y}, \; t = \frac{\partial^2 z}{\partial y^2}. \quad (7)$$

To calculate local morphometric variables, we applied a finite-difference method intended for spheroidal equal angular grids (Florinsky, 1998, 2016, pp. 126–132). Digital models of a nonlocal morphometric variable (i.e., *CA*) were derived from the smoothed DEMs by a method of Martz and de Jong (1988) adapted to spheroidal equal angular grids (Florinsky, 2016, pp. 137–139).

To estimate linear sizes of spheroidal trapezoidal windows in DEM smoothing and morphometric calculation (Florinsky, 2016, pp. 132–133), recommended values of the major and minor semiaxes of the Martian ellipsoid (3,396,190 m and 3,376,200 m – Duxbury et al., 2002) were used for Mars; the Moon was considered as a sphere with the radius of 1,738,000 m. The global DEMs were processed as virtually closed spheroidal matrices of elevations. Each global model included 1,036,800 points (the matrix 1440 × 720).

Then, we visualized global maps of the calculated topographic attributes in the equirectangular projection (Fig. 1). Wide dynamic ranges usually characterize morphometric variables. To avoid loss of information on spatial distribution of their values in mapping, it makes sense to apply a logarithmic transform using the following expression (Shary et al., 2002; Florinsky, 2016, p. 244):

$$\Theta' = sign(\Theta)\ln(1 + 10^n|\Theta|), \quad (8)$$

where Θ and Θ' are an initial and log-transformed values of a morphometric variable, respectively; $n = 0$ for elevation and nonlocal variables, $n = 2, \ldots, 18$ for local variables. Such a form of logarithmic transformation considers that dynamic ranges of some topographic attributes include both positive and negative values. Selection of the n value depends on the grid size; we used $n = 9$.

Data processing was performed by the software LandLord (Florinsky, 2016, p. 413).

2.2. Three-dimensional modeling

To develop the desktop system of virtual morphometric globes, we decided to utilize an existing real-time 3D graphics engine (e.g., Unreal Engine 4 (Epic Games, 2004–2016), Blender 2.76b (Blender Foundation, 2015), and some others). Using a small global DEM of the Earth with the resolution of 30' (Florinsky, 2008a), we analyzed possibilities of such engines constructing of a simple virtual globe. The preference was given to free software with open source and an advanced system of visual logic programming. Finally, we chose the package Blender 2.76b. Its advantages are as follows:

1. It includes a real-time 3D graphics Blender Game Engine (BGE).
2. There are advanced internal facilities for 3D object modeling in Blender.
3. The stability of Blender compared with other graphics engines.
4. The seamless integration of BGE and Blender Editor guarantees accuracy and predictability of 3D models visualized in real-time programs.
5. The Blender's internal programming language is Python, which became in fact the standard language of modern scientific computing.
6. The openness of the Blender source code allows, if necessary, to modify or improve BGE as well as to implement specialized tools in Blender Editor.

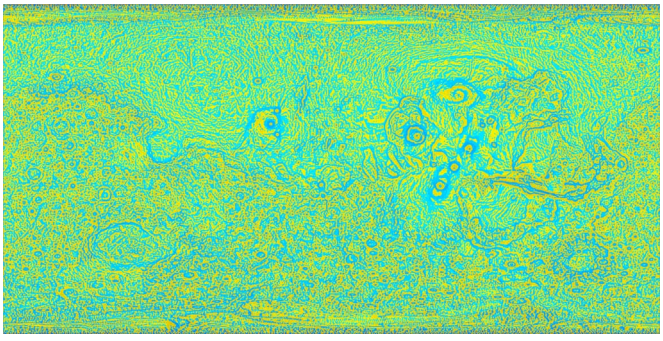

Fig. 1. An example of global morphometric maps: vertical curvature for Mars.

To construct a 3D model of the globe, we selected a UV map of a sphere (U and V are axes of a 2D texture of a 3D object) divided into 1152 rectangular polygons; that is, a sphere tessellated into 48 × 24 spherical trapezoids with sizes of 7.5° × 7.5° (Fig. 2). A reasonably smoothed representation of such a sphere can be achieved using the Phong shading model (Phong, 1975), one of the simplest and most effective algorithms in terms of computing resources.

Global morphometric maps, presented in the equirectangular projection and saved in the TIFF format (Fig. 1), were superimposed to the sphere as textures influencing the *Color* and *Emit* channels, responsible for the color and luminosity of an object. It was done to avoid (1) glares on the surface of the globe, and (2) need for light sources traditionally complicating real-time rendering of the scenes.

To create a latitude/longitude grid on the globe, we used a UV map of such a grid with the grid size of 7.5°. The UV map was imposed to the sphere surface, over a morphometric texture, as the second, semi-transparent texture.

The globe rotation was performed using the *Mouse* actuator (the *Look* mode) embedded in BGE. Two mouse sensors (*Mouse Event Movement* and *Mouse Event Left Button*) were linked by the *And* controller. The globe rotation was also implemented using cursor movement keys of the keyboard.

The scaling (zooming) of the globe was performed using both mouse and keyboard. The BGE camera was connected with two logical chains including two mouse sensors (*Mouse Wheel Down* and *Mouse Wheel Up*) as well as two key sensors (*Numpad+* and *Numpad–*). They were linked with the *Motion* actuators providing the BGE camera motion along the Y-axis (Fig. 3).

All morphometric globes were generated as individual scenes within a project of the Blender Editor. To switch between scenes, a corresponding logic was created including a main menu. Finally, the Blender project was assembled into a standalone desktop program using the Blender standard tools (saved as Game Engine Runtime).

3. Results and discussion

Figs. 4 and 5 show examples (screenshots) of the developed morphometric globes for Mars and the Moon. In both cases, the scene screenshots were made for the same position of the six globes relative to the observer.

For Mars (Fig. 4), one can see most of the Western hemisphere, including the Tharsis region (Tharsis Montes, Alba Mons, Daedalia Planum, Syria Planum) and Olympus Mons in the central and lower parts of the scenes; Amazonis and Arcadia Planitias in the left part of the scenes; a western portion of Vastitas Borealis in the upper part of the scenes; Tempe Terra, Echus Chasma, Valles Marineris, and Solis

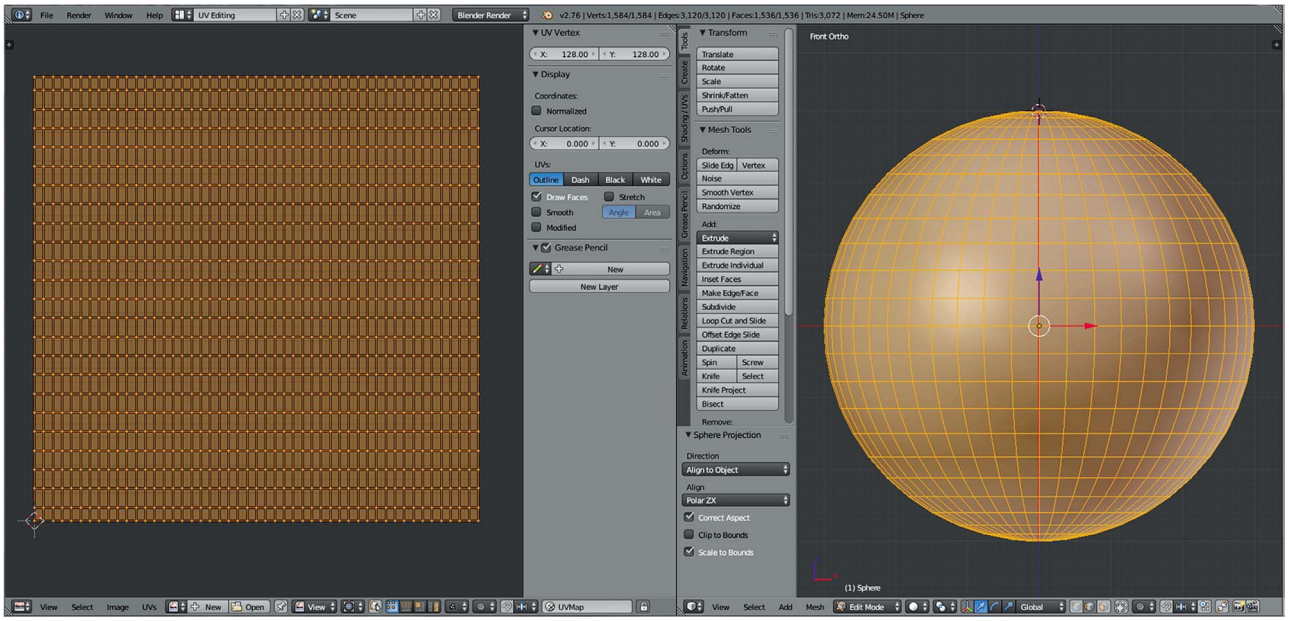

Fig. 2. A geometric model for a virtual globe: UV-map of a sphere (left) and 3D model of a sphere (right).

Planum in the right part of the scenes; as well as a northern portion of Terra Sirenum in left lower part of the scenes.

For the Moon (Fig. 5), one can see a south-western portion of the Near side in the central, right, upper and lower parts of the scenes. Also, a small southeastern portion of the Far side can be seen in the left part of the scenes. In particular, these include Oceanus Procellarum, Mares

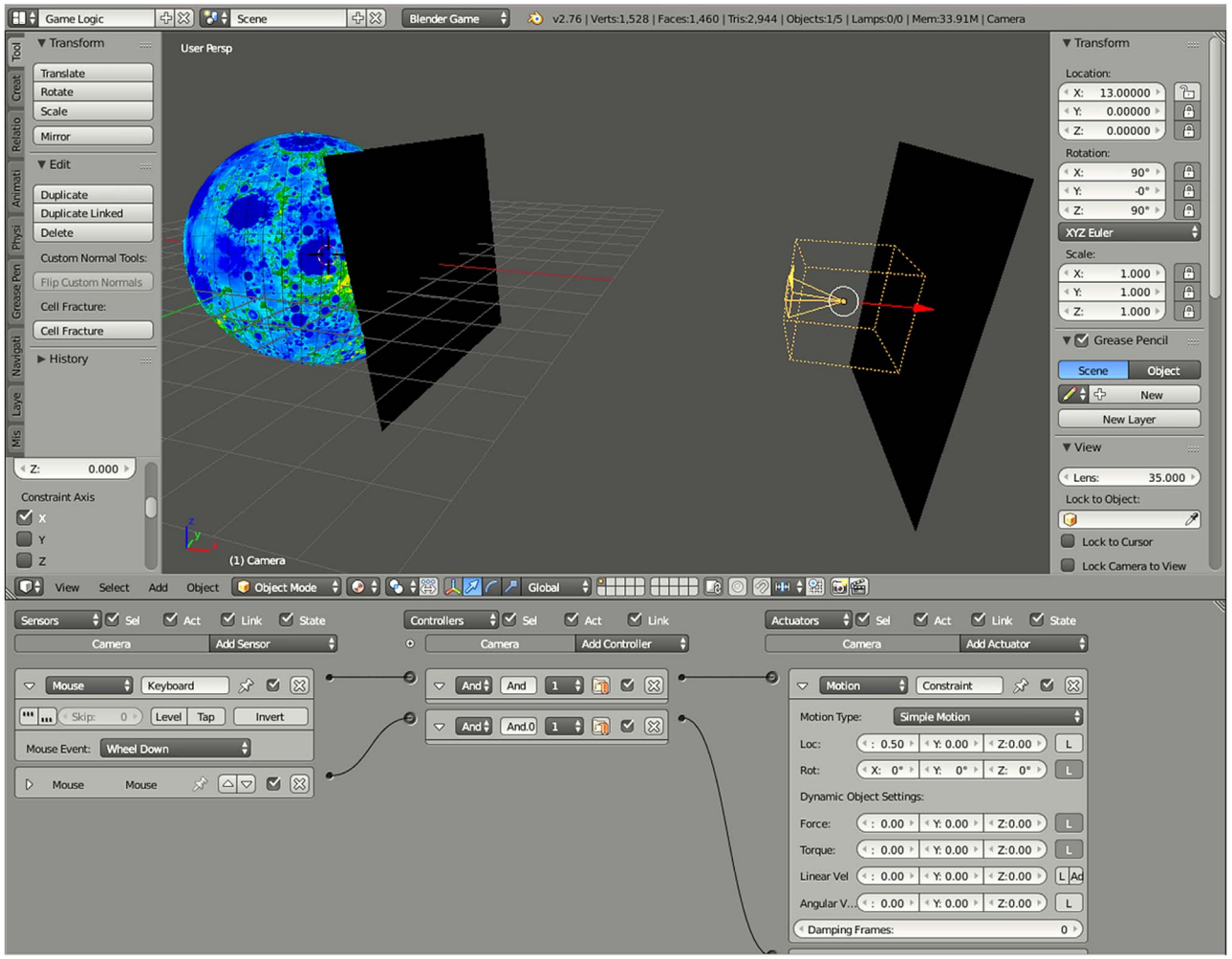

Fig. 3. The general view of a scene (upper) and the logic of zooming (lower).

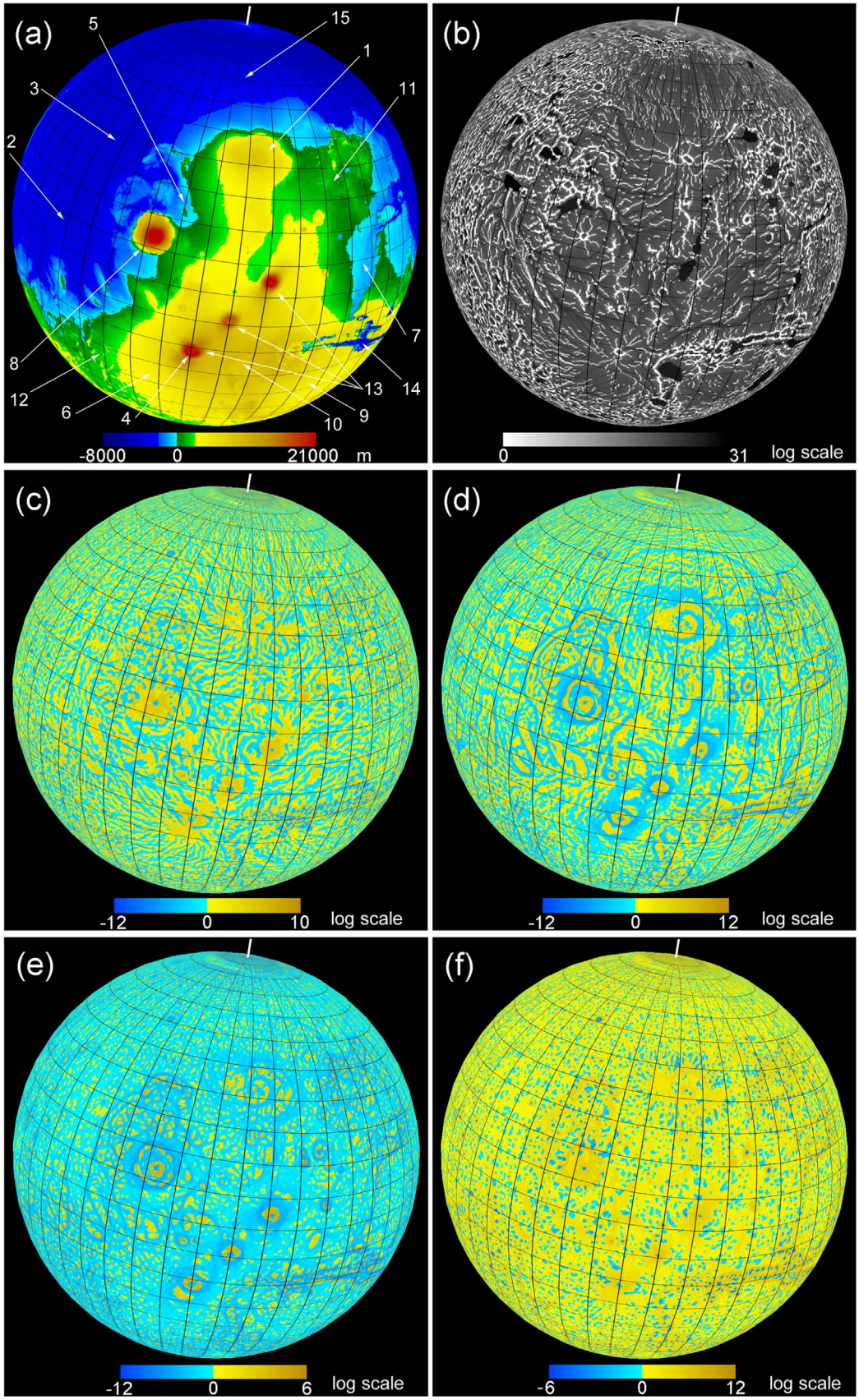

Fig. 4. Mars, morphometric globes: (a) elevation, (b) catchment area, (c) horizontal curvature, (d) vertical curvature, (e) minimal curvature, and (f) maximal curvature. The places cited in the text are indicated on the elevation scene as follows: 1 – Alba Mons, 2 – Amazonis Planitia, 3 – Arcadia Planitia, 4 – Arsia Mons, 5 – Cyane Fossae, 6 – Daedalia Planum, 7 – Echus Chasma, 8 – Olympus Mons, 9 – Solis Planum, 10 – Syria Planum, 11 – Tempe Terra, 12 – Terra Sirenum, 13 – Tharsis Montes, 14 – Valles Marineris, 15 – Vastitas Borealis.

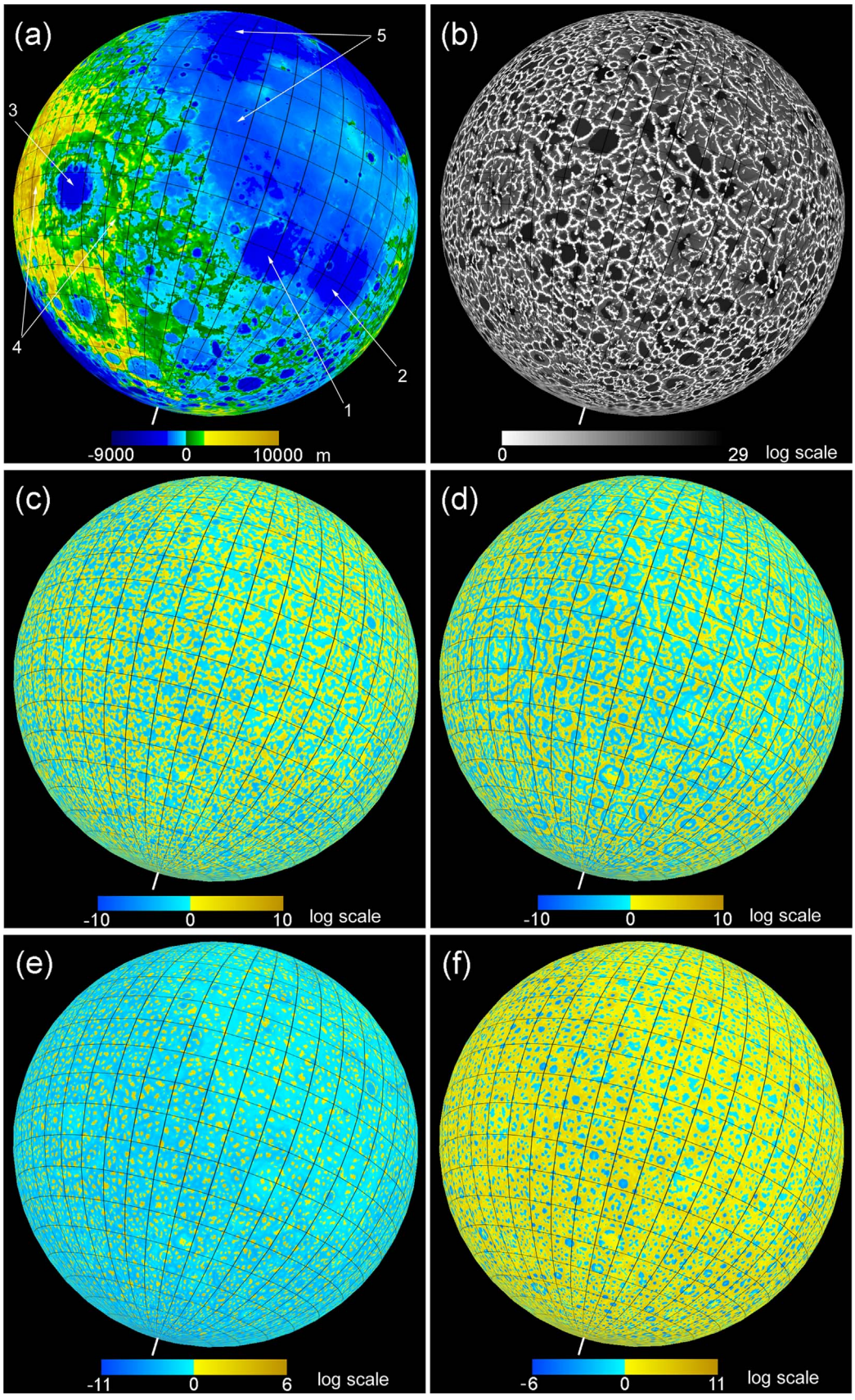

Fig. 5. The Moon, morphometric globes: (a) elevation, (b) catchment area, (c) horizontal curvature, (d) vertical curvature, (e) minimal curvature, and (f) maximal curvature. The places cited in the text are indicated on the elevation scene as follows: 1 – Mare Humorum, 2 – Mare Nubium, 3 – Mare Orientale, 4 – Montes Cordillera, 5 – Oceanus Procellarum.

Humorum and Nubium, Montes Cordillera, Mare Orientale, and many smaller craters.

Morphometric globes clearly represent peculiarities of planetary topography, according to the physical and mathematical sense of a particular morphometric variable, so these globes complement each other. For example, catchment area (Table 1) measures an upslope area potentially drained through a point on the topographic surface. On the *CA* globe of Mars (Fig. 4b), the planetary network of ridges is delineated by low values of *CA* as white lines, while valleys and canyons are delineated by high values of *CA* as black lines; depressions (basins) are represented as dark areas (high values of *CA*). Calderas of large volcanoes (e.g., Tharsis Montes, Alba Mons, and Olympus Mons) are revealed as dark areas (high values of *CA* indicating depressions) surrounded by white 'rings' (low values of *CA* indicating circular crests). Impact craters are similarly delineated on the *CA* globe of the Moon (Fig. 5b).

Horizontal curvature (Table 1) delineates areas of flow divergence and convergence (positive and negative values, yellow and blue patterns, correspondingly), which form so-called flow structures. On the k_h globe of Mars (Fig. 4c), one can see several huge, fan-like systems of flow structures. Three of them begin on the northern, western, and southern slopes of Alba Mons. They go north to Vastitas Borealis, west to Arcadia Planitia, and southwest to Cyane Fossae trough between Alba and Olympus Montes. Another one system of flow structures begins on the southern and western slopes of Arsia Mons (the southernmost of the three Tharsis Montes) and goes south to Daedalia Planum as well as west and northwest to the Amazonis Planitia. For the Moon, the k_h globe (Fig. 5c) represents cell-like patterns resulting from a predominance of craters at the global scale.

Vertical curvature (Table 1) measures relative acceleration and deceleration of flows (positive and negative values, yellow and blue patterns, correspondingly). Geomorphologically, k_v delineates escarps, terraces, and similar features. On the k_v globe of Mars (Fig. 4d), one can particularly see the eastern cliff-like boundary of Amazonis Planitia, escarpments of Olympus, Alba, and Tharsis Montes, as well as a system of terrace-like features in the northern part of Vastitas Borealis. These features relate to northern margin of the fan-like system of flow structures beginning on the northern slopes of Alba Mons (see above). On the k_v globe of the Moon (Fig. 5d), ring mountains of craters are delineated including three concentric rings of mountains around the basin of Mare Orientale.

Minimal curvature (Table 1) reveals local convex landforms, such as 'hills' (positive values, yellow patterns) and elongated concave landforms, such as troughs (negative values, blue patterns) (Figs. 4e and 5e). Maximal curvature (Table 1) reveals local concave landforms, such as small impact basins (negative values, blue patterns) and elongated convex landforms (positive values, yellow patterns) (Figs. 4f and 5f).

For the same angular resolution of 15', morphometric globes of Mars and the Moon have distinct linear resolution (around 14.8 km and 7.6 km on the equator, correspondingly).

Accuracy of morphometric models depends on (a) the spatial distribution of errors in the initial DEMs, and (b) properties of computation methods. Derivation of local morphometric variables (e.g., curvatures) is based on calculations of the partial derivatives of elevation. These calculations significantly amplify random errors (or high-frequency noise) in DEMs. Derivation of nonlocal morphometric variables (e.g., catchment area) is based on flow-routing algorithms. During these computations, errors are accumulated along flow routes depending on the spatial distribution of random and systematic errors in a DEM.

Morphometric variables are functions of measured variables (viz., elevations). Thus, to estimate the accuracy of morphometric models, one can use a criterion of root mean square error of a function of measured variables (RMSE-FMV). To describe and analyze accuracy of morphometric models, one can produce RMSE-FMV models. However, this issue is beyond the scope of this paper; details can be found elsewhere (Florinsky, 1998, 2016, pp. 162–163).

4. Conclusions

We developed the desktop system of virtual morphometric globes for Mars and the Moon. The system was constructed using Blender, the open-source software for 3D modeling, visualization, and animation. The real-time testing of the developed system demonstrated its good performance.

The desktop system is rather simple: (1) data on only six morphometric variables are represented; (2) morphometric models and textures of low resolution — 15' — are used; and (3) this is a desktop software. However, we believe that virtual morphometric globes, even in the current simplified form, can be used for some small-scale planetary studies.

In a next, web version of the system, we plan: (1) to incorporate data on a representative set of morphometric variables (up to 17 variables); (2) to use morphometric textures of higher resolution (up to 30"); (3) to apply a hierarchical tessellation of the globe surface; and (4) to provide free, real-time web access to the system. The web system of virtual morphometric globes will be designed as a separate unit of a 3D web GIS for storage and access to planetary data (Garov et al., 2016), which is currently developed as an extension of an existing 2D web GIS (MExLab, 2012–2016).

Similar morphometric globes can be also developed for other celestial bodies of the Solar system, for which global DEMs are available (e.g., Venus, Mercury, and Phobos).

Acknowledgements

The study was supported by the Russian Foundation for Basic Research, grant 15-07-02484.

References

AGI, 2012–2015. Cesium. Exton, PA: Analytical Graphics, Inc., ⟨https://cesium.agi.com⟩.
Autin, L., et al., 2012. uPy: a ubiquitous CG Python API with biological-modeling applications. IEEE Comput. Graph. Appl. 32 (5), 50–61. http://dx.doi.org/10.1109/MCG.2012.93.
Blain, J.M., 2014. The Complete Guide to Blender Graphics: Computer Modeling and Animation 2nd ed. CRC Press, Boca Raton, FL.
Blaschke, T., et al., 2012. Virtual globes: serving science and society. Information 3 (3), 372–390. http://dx.doi.org/10.3390/info3030372.
Blender Foundation, 2003–2015. Blender. Amsterdam: Stichting Blender Foundation, ⟨https://www.blender.org⟩.
Cazenave, A., Souriau, A., Dominh, K., 1989. Global coupling of Earth surface topography with hotspots, geoid and mantle heterogeneities. Nature 340 (6228), 54–57. http://dx.doi.org/10.1038/340054a0.
Chen A. and Bailey J. (Eds.), Virtual globes in science. *Computers and Geosciences*, 37 (1), 2011, 1–110.
Cozzi, P., Ring, K., 2011. 3D Engine Design for Virtual Globes. A K Peters/CRC Press, Boca Raton, FL.
Duxbury, T., Kirk, R., Archinal, B., Neumann, G., 2002. Mars Geodesy/Cartography working group recommendations on Mars cartographic constants and coordinate systems. ISPRS Arch. 34 (4), 4.
Epic Games, 2004–2016. Unreal Engine 4. Cary, NC: Epic Games Inc., ⟨https://www.unrealengine.com⟩.
Evans, I.S., 1972. General geomorphometry, derivations of altitude, and descriptive statistics. In: Chorley, R.J. (Ed.), Spatial Analysis in Geomorphology. Methuen, London, 17–90.
Fillipov, S.V., Sobolev, E.V., 2002. Using techniques of professional computer graphics to visualize results of scientific research. In: Lakhno, V.D., Ustinin, M.N. (Eds.), Computers and Supercomputers in Biology. Institute of Computer Research, Izhevsk (in Russian), 476–497.
Florinsky, I.V., 1998. Derivation of topographic variables from a digital elevation model given by a spheroidal trapezoidal grid. Int. J. Geogr. Inf. Sci. 12 (8), 829–852. http://dx.doi.org/10.1080/136588198241527.
Florinsky, I.V., 2002. Errors of signal processing in digital terrain modelling. Int. J. Geogr. Inf. Sci. 16 (5), 475–501. http://dx.doi.org/10.1080/13658810210129139.
Florinsky, I.V., 2008a. Global lineaments: application of digital terrain modelling. In: Zhou, Q., Lees, B., Tang, G.-A. (Eds.), Advances in Digital Terrain Analysis. Springer, Berlin, 365–382. http://dx.doi.org/10.1007/978-3-540-77800-4_20.
Florinsky, I.V., 2008b. Global morphometric maps of Mars, Venus, and the Moon. In: Moore, A., Drecki, I. (Eds.), Geospatial vision: New Dimensions in Cartography. Springer, Berlin, 171–192. http://dx.doi.org/10.1007/978-3-540-70970-1_8.
Florinsky, I.V., 2016. Digital Terrain Analysis in Soil Science and Geology 2nd ed. Academic Press, Amsterdam.

Garov, A.S., et al., 2016. Development of a heterogenic distributed environment for spatial data processing using cloud technologie. Int. Arch. Photogramm., Remote Sens. Spat. Inf. Sci. 41 (B4), 385–390. http://dx.doi.org/10.5194/isprs-archives-XLI-B4-385-2016.

Google, 2005–2014. Google Earth. Google Inc., ⟨http://www.google.com/earth⟩.

Graham, S.T., Famiglietti, J.S., Maidment, D.R., 1999. Five-minute, 1/2°, and 1° data sets of continental watersheds and river networks for use in regional and global hydrologic and climate system modeling studies. Water Resour. Res. 35 (2), 583–587. http://dx.doi.org/10.1029/1998WR900068.

Gunia, D.A., 2004–2015. Earth3D, ⟨http://www.earth3d.org⟩.

Guth, P.L., 2012. Automated export of GIS maps to Google Earth: tool for research and teaching. Geol. Soc. Am. Spec. Pap. 492, 165–182. http://dx.doi.org/10.1130/2012.2492(12).

C.D. Hansen, C.R. Johnson (Eds.) The Visualization Handbook, 2005, Academic Press Amsterdam.

T. Hengl, H.I. Reuter (Eds.) Geomorphometry: Concepts, Software, Applications, 2009, Elsevier Amsterdam

Hess, R., 2010. Blender Foundations: The Essential Guide to Learning Blender 2.6. Focal Press, Amsterdam.

Horn, B.K.P., 1981. Hill shading and the reflectance map. Proc. IEEE 69 (1), 14–47. http://dx.doi.org/10.1109/PROC.1981.11918.

Jenny, B., Hurni, L., 2006. Swiss-style colour relief shading modulated by elevation and by exposure to illumination. Cartogr. J. 43 (3), 198–207. http://dx.doi.org/10.1179/000870406×158164.

Johnson, G.T., Hertig, S., 2014. A guide to the visual analysis and communication of biomolecular structural data. Nat. Rev. Mol. Cell Biol. 15 (10), 690–698. http://dx.doi.org/10.1038/nrm3874.

Karachevtseva, I.P., et al., 2014. The Phobos information system. Planet. Space Sci. 102, 74–85. http://dx.doi.org/10.1016/j.pss.2013.12.015.

Karachevtseva, I., et al., 2015. Development of a new Phobos atlas based on Mars Express image data. Planet. Space Sci. 108, 24–30. http://dx.doi.org/10.1016/j.pss.2014.11.024.

KDE, 2007–2014. Marble. Berlin: K Desktop Environment, ⟨https://marble.kde.org⟩.

Kennedy, K.H., 2009. Introduction to 3D Data: Modeling with ArcGIS® 3D Analyst™ and Google Earth™. Wiley, Hoboken, NJ.

Kent, B.R., 2013. Visualizing astronomical data with Blender. Publ. Astron. Soc. Pac. 125 (928), 731–748. http://dx.doi.org/10.1086/671412.

Kent, B.R., 2015. 3D Scientific Visualization with Blender®. Morgan & Claypool Publishers, San Rafael, CA.

Li, Z., Zhu, Q., Gold, C., 2005. Digital Terrain Modeling: Principles and Methodology. CRC Press, New York.

Lipşa, D.R., et al., 2012. Visualization for the physical sciences. Comput. Graph. Forum 31 (8), 2317–2347. http://dx.doi.org/10.1111/j.1467-8659.2012.03184.x.

Mahdavi-Amiri, A., Alderson, T., Samavati, F., 2015. A survey of Digital Earth. Comput. Graph. 53 (B), 95–117. http://dx.doi.org/10.1016/j.cag.2015.08.005.

Martz, L.W., de Jong, E., 1988. CATCH: a FORTRAN program for measuring catchment area from digital elevation models. Comput. Geosci. 14 (5), 627–640. http://dx.doi.org/10.1016/0098-3004(88)90018-0.

MExLab, 2012–2016. Planetary Geoportal. Moscow: MIIGAiK Extraterrestrial Laboratory, Moscow State University of Geodesy and Cartography (MIIGAiK), ⟨http://cartsrv.mexlab.ru/geoportal⟩.

Moore, I.D., Grayson, R.B., Ladson, A.R., 1991. Digital terrain modelling: a review of hydrological, geomorphological and biological applications. Hydrol. Process. 5 (1), 3–30. http://dx.doi.org/10.1002/hyp.3360050103.

Müller, R.D., et al., 2016. The GPlates portal: cloud-based interactive 3D visualization of global geophysical and geological data in a web browser. PLoS ONE 11 (3), e0150883. http://dx.doi.org/10.1371/journal.pone.0150883.

NASA, 2003–2011. NASA World Wind. National Aeronautics and Space Administration, ⟨http://worldwind.arc.nasa.gov⟩.

Neumann, G.A., 2008. Lunar Reconnaissance Orbiter LOLA Instrument Science Data Archive. NASA PDS Geosciences Node, Washington University, St. Louis, MO⟨http://pds-geosciences.wustl.edu/missions/lro/lola.htm⟩.

Paraskevas, T., 2011. Virtual globes and geological modeling. Int. J. Geosci. 2, 648–656. http://dx.doi.org/10.4236/ijg.2011.24066.

Phong, B.T., 1975. Illumination for computer generated pictures. Commun. ACM 18 (6), 311–317. http://dx.doi.org/10.1145/360825.360839.

Scianna, A., 2013. Building 3D GIS data models using open source software. Appl. Geomat. 5 (2), 119–132. http://dx.doi.org/10.1007/s12518-013-0099-3.

SciVis, 2011–2015. BioBlender. Pisa, Italy: Scientific Visualization Unit, Institute of Clinical Physiology – CNR, ⟨http://www.bioblender.eu⟩.

Scheffers, A.M., May, S.M., Kelletat, D.H., 2015. Landforms of the World with Google Earth: Understanding Our Environment. Springer, Dordrecht.

Shary, P.A., Sharaya, L.S., Mitusov, A.V., 2002. Fundamental quantitative methods of land surface analysis. Geoderma 107 (1–2), 1–32. http://dx.doi.org/10.1016/S0016-7061(01)00136-7.

Smith, D.E., et al., 1999. The global topography of Mars and implications for surface evolution. Science 284 (5419), 1495–1503. http://dx.doi.org/10.1126/science.284.5419.1495.

Smith, D.E., et al., 2003. Mars Global Surveyor Laser Altimeter Mission Experiment Gridded Data Record. NASA Planetary Data System Geosciences Node, Washington University, St. Louis, MO⟨http://pds-geosciences.wustl.edu/missions/mgs/megdr.html⟩.

Smith, D.E., et al., 2010. Initial observations from the Lunar Orbiter Laser Altimeter. Geophys. Res. Lett. 37, L18204. http://dx.doi.org/10.1029/2010GL043751.

Solomon, S.C., et al., 1991. Venus tectonics: initial analysis from Magellan. Science 252 (5003), 297–312. http://dx.doi.org/10.1126/science.252.5003.297.

Tuttle, B.T., Anderson, S., Huff, R., 2008. Virtual globes: an overview of their history, uses, and future challenges. Geogr. Compass 2 (5), 1478–1505. http://dx.doi.org/10.1111/j.1749-8198.2008.00131.x.

Vörösmarty, C.J., et al., 2000. Geomorphometric attributes of the global system of rivers at 30-minute spatial resolution. J. Hydrol. 237 (1–2), 17–39. http://dx.doi.org/10.1016/S0022-1694(00)00282-1.

Wählisch, M., et al., 2014. Phobos and Deimos cartography. Planet. Space Sci. 102, 60–73. http://dx.doi.org/10.1016/j.pss.2013.05.012.

Whitmeyer,, S.J. (Ed.), 2012. Google Earth and Virtual Visualizations in Geoscience Education and Research. Geological Society of America, Boulder, CO.

Wieczorek, M.A., 2007. Gravity and topography of the terrestrial planetsTreatise on Geophysics 10. Elsevier, Amsterdam, 165–206. http://dx.doi.org/10.1016/B978-044452748-6.00156-5.

Willner, K., Shi, X., Oberst, J., 2014. Phobos' shape and topography models. Planet. Space Sci. 102, 51–59. http://dx.doi.org/10.1016/j.pss.2013.12.006.

Wilson, J.P., Gallant, J.C. (Eds.), 2000. Terrain Analysis: Principles and Applications. Wiley, New York.

Yu, L., Gong, P., 2012. Google Earth as a virtual globe tool for Earth science applications at the global scale: progress and perspectives. Int. J. Remote Sens. 33 (12), 3966–3986. http://dx.doi.org/10.1080/01431161.2011.636081.

Zhu, L., Pan, X., Sun, J., 2016. Visualization and dissemination of global crustal models on virtual globes. Comput. Geosci. 90 (A), 34–40. http://dx.doi.org/10.1016/j.cageo.2016.01.015.

Zhu, L., et al., 2014. SolidEarth: a new Digital Earth system for the modeling and visualization of the whole Earth space. Front. Earth Sci. 8 (4), 524–539. http://dx.doi.org/10.1007/s11707-014-0438-7.